Transient interactions between photosynthetic proteins

Hulsker, R.

Chapter IV

Dynamics in the complex of *Nostoc* sp. PCC 7119 cytochrome c_6-cytochrome *f*

Abstract

The role of electron carrier between cyt*f* and PSI can be carried out by Pc and cytc_6. A docking model for the physiological cytc_6 – cyt*f* complex from *Nostoc* sp. PCC 7119 based on chemical shift perturbations revealed that the orientation of cytc_6 in the complex is similar to the orientation of Pc in the Pc - cyt*f* complex. Additional information from pseudocontact shifts (PCS) and paramagnetic relaxation enhancement (PRE) has been used to investigate the structure and dynamics of this complex. Including PCS data into docking calculations leads to a single structure which has a similar orientation to the structure from chemical shift data only. When PRE from five different spin labels on the surface of cyt*f* are used in docking, single structures are also found, but with different orientations depending on which combination is used. Furthermore, the violations for each of the structures determined remain large, especially for the spin label furthest away from the site of electron transfer. This suggests that the complex is dynamic and cannot be described by a single structure. Simulation of dynamics in the complex by creating an ensemble of structures around the structure determined by chemical shift perturbations and PCS (or by chemical shift perturbations alone) as described in Chapter III did not reduce the violations of the distances derived from PRE. This shows that the complex of cytc_6 and cyt*f* cannot be described by a single model of stochastic excursions from a single structure. Most likely, cytc_6 has multiple preferred orientations.

The results in this chapter will be published as:
The structure and dynamics in the complex of *Nostoc* sp. PCC 7119 cytochrome *f*-cytochrome c_6 (manuscript in preparation).

Introduction

During oxygenic photosynthesis electrons are shuttled between the cytochrome b_6f complex and PSI by a mobile electron carrier. In plants this role is performed by the copper protein Pc, while in some cyanobacteria and algae cytc_6 is produced instead. Other photosynthetic organisms adapt to the copper and iron availability in their environment by producing either of the two proteins[111]. While the complex between Pc and cyt*f* has been well characterised, only a limited amount of studies have been done on the cytc_6 - cyt*f* complex. The first clues on the binding characteristics were found in an NMR study on the non-physiological cyanobacterial complex of cyt*f* from *Ph. laminosum* and cytc_6 from *Nostoc* sp. PC 7119 (former *A. variabilis*)[136]. This revealed a binding interface typical of electron transfer proteins and suggested it is a well-defined complex. More information on the behaviour of cytc_6 in a physiological transient complex comes from its interaction with PSI[212]. It was found that hydrophobic and electrostatic patches, which surround the haem cleft of cytc_6, are affected by binding. These patches had been identified before by site-directed mutagenesis studies[213,214]. Recently, a docking model for the physiological cytc_6 – cyt*f* complex from *Nostoc* sp. PC 7119 based on chemical shift perturbations was reported[135]. It revealed that the orientation of cytc_6 in the complex is reminiscent of the orientation of Pc in the Pc - cyt*f* complex from the same species. As described in Chapter III, and from other recent studies[31,188], additional NMR data such as pseudocontact shifts (PCS) and paramagnetic relaxation enhancement (PRE) can provide insight into the dynamics of transient protein-protein complexes. Here, we describe an attempt to combine these approaches to resolve the dynamics in the *Nostoc* sp. PC 7119 cytc_6 – cyt*f* complex.

Materials and Methods

Protein preparation

Uniformly ^{15}N-labelled M58C cytc_6 was kindly provided by Dr. Fernando Molina-Heredia and Prof. Miguel A. De la Rosa (Seville, Spain). *E. coli* cell pellets containing cyt*f* 'Cys' variants were kindly provided by Michela Finiguerra (Leiden, the Netherlands). Cells were resuspended in the minimal volume of buffer (5 mM TRIS pH 8.0, 3 mM DTT), followed by addition of 5 mg DNase and lysozyme and 1 mM PMSF. Extracts of the harvested cells were obtained through use of the French press cell. Cell debris was removed by ultra-centrifugation at 30.000 rpm after which the supernatant was dialysed against 5 L of 5 mM TRIS pH 8.0, 3 mM DTT for 3 hours and overnight at 4°. Cyt*f* was purified using ion exchange chromatography with DEAE sepharose (Amersham Biosciences) in 5 mM TRIS pH 8.0, 3 mM DTT. The protein was eluted with a gradient of 0-500 mM NaCl. The fractions containing cyt*f* were concentrated and size exclusion chromatography was performed with Superdex-G75 (Amersham Pharmacia Biotech) in 5 mM TRIS pH 8.0, 3 mM DTT, 100 mM NaCl. DTT was removed from cyt*f* solutions by ultrafiltration (Amicon, MW cut-off 10 kDa). The protein was subsequently exchanged to 10 mM NaPi, pH 6.0 and concentrated to ~40 μM. The protein was oxidised by a 100-fold excess of $K_3[Fe(CN)_6]$ and a 10-fold excess of either MTSL or MTS was added. MTSL [(1-oxyl-2,2,5,5-tetramethyl-3-pyrroline-3-methyl)-methanethiosulfonate] and MTS [(1-acetyl-2,2,5,5-tetramethyl-3-pyrroline-3-methyl)-methanethiosulfonate] were purchased from Toronto Research Chemicals (North York, Ontario, Canada) and used without further purification. Stock solutions of 0.1 M MTS(L) in DMSO were used. The protein solution was kept for 2 hours at RT and O/N at 4° after which the excess $K_3[Fe(CN)_6]$ and MTS(L) was removed by ultrafiltration. Modification of cyt*f* with MTS(L) was confirmed by mass spectroscopy and an estimate of the labelling ratio was made from EPR experiments[31].

NMR experiments

All samples contained 10 mM NaPi, pH 6.0 and 6% D_2O. Protein concentrations were determined by optical spectroscopy using ε_{419} of 85.5 mM^{-1} cm^{-1} for M58C cytc_6 and ε_{556} of 31.5 mM^{-1} cm^{-1} for reduced cyt$f$ [215]. The pH was adjusted with µL aliquots of 0.1/0.5 M HCl. The concentration of cyt*f*-MTS or cyt*f*-MTSL stock solutions was carefully set to 0.7 mM. Samples contained 0.3 mM ^{15}N M58C cytc_6 and 0.1 mM cyt*f*-MTS or cyt*f*-MTSL. The diamagnetic and paramagnetic experiments were performed on cytc_6 from the same stock solution. All NMR spectra were recorded at 300 K on a Bruker DMX600 spectrometer equipped with a triple-resonance TCI-ZGRAD ATM Cryoprobe (Bruker, Karlsruhe, Germany). ^{15}N,^{1}H HSQC were obtained with spectral widths of 32 ppm (^{15}N) and 13.5 ppm (^{1}H) and 1024 and 256 complex points were acquired in the direct and indirect dimension, respectively. Data were processed with AZARA 2.7 [203] and analysed in ANSIG for Windows[204]. Sequence specific assignments of the backbone resonances of M58C cytc_6 were kindly provided by Dr. Irene Díaz-Moreno (Seville, Spain).

Determination of distance restraints (PRE)

From the intensities of the recorded M58C cytc_6 resonances the paramagnetic relaxation enhancement (PRE) effects were calculated using equation 4a [52]:

$$\frac{I_{para}}{I_{dia}} = \frac{R_{2,dia}\exp(-tR_{2,para})}{R_{2,dia}+R_{2\,para}} \qquad (4a)$$

where I_{para} and I_{dia} are the intensities of the ^{15}N M58C cytc_6 peaks in the presence of cyt*f*-MTSL and cyt*f*-MTS, respectively; $R_{2,dia}$ is the transverse relaxation rate of M58C cytc_6 backbone amides in the presence of cyt*f*-MTS ; $R_{2,para}$ is the paramagnetic contribution to the relaxation rate (PRE) and t is the INEPT evolution time of the recorded HSQC (9 ms). For residues of which the resonances disappear from the spectrum, the maximal intensity was estimated from the noise level. These residues were classified in the 'upper limit' distance class for docking calculations (see below).

The $R_{2,dia}$ values were determined from the peaks in the HSQC spectrum of M58C cytc_6 in the presence of cyt*f*-MTS. For this purpose the FIDs were zero-filled up to 2048 and

512 complex points in the direct and indirect dimension, respectively. The resulting FIDs were multiplied with a 2 Hz line-broadening single exponential window function in the ^{1}H dimension. The width at half-height ($\Delta\nu_{1/2}$) of each peak was determined from a Lorentzian fit performed in the program MestRe-C 4.8.6.0 (Mestrelab Research S.L., Santiago de Compostela, Spain). After correction for artificial line-broadening the $R_{2,dia}$ was calculated ($R_{2,dia} = \pi\Delta\nu_{1/2}$) and converted into distances using equation 4b [52]:

$$r = \sqrt[6]{\frac{\gamma^2 g^2 \beta^2 \tau_c}{20 R_{2,para}} \left(4 + \frac{3}{1+\omega_h^2 \tau_c^2} \right)} \qquad (4b)$$

where r is the distance of the amide proton in M58C cytc_6 to the spin label (attached to cyt*f*); γ is the gyromagnetic ratio of ^{1}H; g is electronic g-factor; β is the Bohr magneton; ω_h is the ^{1}H Larmor frequency and τ_c is the correlation time of the electron-nucleus vector. The τ_c values used for the five positions of the MTSL on cyt*f* were 6 ns for Q7C, 14 ns for A63C, 6 ns for N71C, 3 ns for Q104C and 7 ns for S192C. These values were derived from EPR spectra on the cyt*f* – cytc_6 complexes and were kindly provided by Francesco Scarpelli and Dr. Martina Huber (Leiden, the Netherlands).

From the K_a of (6.5 ± 0.7) x 10^3 M^{-1} it was calculated that the fraction bound in the NMR samples with 1:1 stoichiometry of cytc_6 – cyt*f* is 25%. The $R_{2,para}$ was multiplied with a factor of 1/0.25 because the observed PRE's represent this fraction of the total PRE. The distances calculated from the PRE were divided into three classes. The resonances that disappeared from the spectrum were included in an upper limit restraint class. Resonances that experienced an intensity change of less than 10% were included in a minimal distance restraint class (lower limit). A two-bounds class included the resonances that experience more than 10% of intensity change, but are still observed. A summary of the restraints is given in Table 4.1.

Table 4.1. Number of distance restraints for each spin label on cyt*f*.

Spin label	Upper bound	Lower bound	2-bound	Total
Q7C	2	54	34	90
A63C	10	49	29	88
N71C	11	38	40	89
Q104C	10	53	25	88
S192C	2	67	18	87

Docking with PRE restraints

The XRD structure of M58C cytc_6 was determined by Dr. Navraj Pannu and Prof. Jan Pieter Abrahams (Leiden, the Netherlands) from crystals prepared by Davide Cavazzini and Prof. Gian Luigi Rossi (Parma, Italy). Coordinates of cyt*f* from a previously described homology model[109] were used. Modifications of the model in order to add the MTSL atoms were performed by Dr. Alexander N. Volkov (Louvain-la-Neuve, Belgium) as described[31]. The five cysteine surface mutations were introduced *in silico* and four orientations representative of all sterically allowed orientations per MTSL spin label were added to account for its mobility[55]. Docking of M58C cytc_6 onto cyt*f* was done using restrained rigid body molecular dynamics in XPLOR-NIH 2.9.9 [208]. The coordinates of cyt*f* were fixed, while M58C cytc_6 was placed at a random position and allowed to move under the forces of restraints and a van der Waals repel function. The restraint for a particular residue was defined as the r^{-6} averaged distance between the O atoms of the representative spin label orientations and the amide protons.

Dynamics simulations

Dynamics in the M58C cytc_6 – cyt*f* complex was simulated in XPLOR-NIH 2.9.9 [208] as described in Chapter III [216]. The initial orientation of the complex was identical to either the published structure determined by docking with restraints derived from chemical shift changes[135] only, or the structure determined by docking with restraints from both chemical shift changes and PCS. Both the structures and PCS data for comparison were kindly provided by Dr. Irene Díaz-Moreno (Seville, Spain).

Results and Discussion

Paramagnetic effects in the ^{15}N M58C cytc$_6$ – cytf-MTSL complex

To characterise the dynamics in the physiological complex between cytc_6 and cyt*f* from cyanobacterium *Nostoc* sp. PCC 7119 a series of paramagnetic spin labels was attached to cyt*f*. For this purpose five surface-exposed cyt*f* residues were singly mutated to cysteines (Finiguerra M.G. *et al*., in preparation), to which a thiol-specific paramagnetic spin label (MTSL) was subsequently connected. The selected positions of the spin labels on the surface of cyt*f* are close to the haem, the site of electron transfer, except S192C, which is positioned on the small domain of cyt*f* (Fig. 4.1).

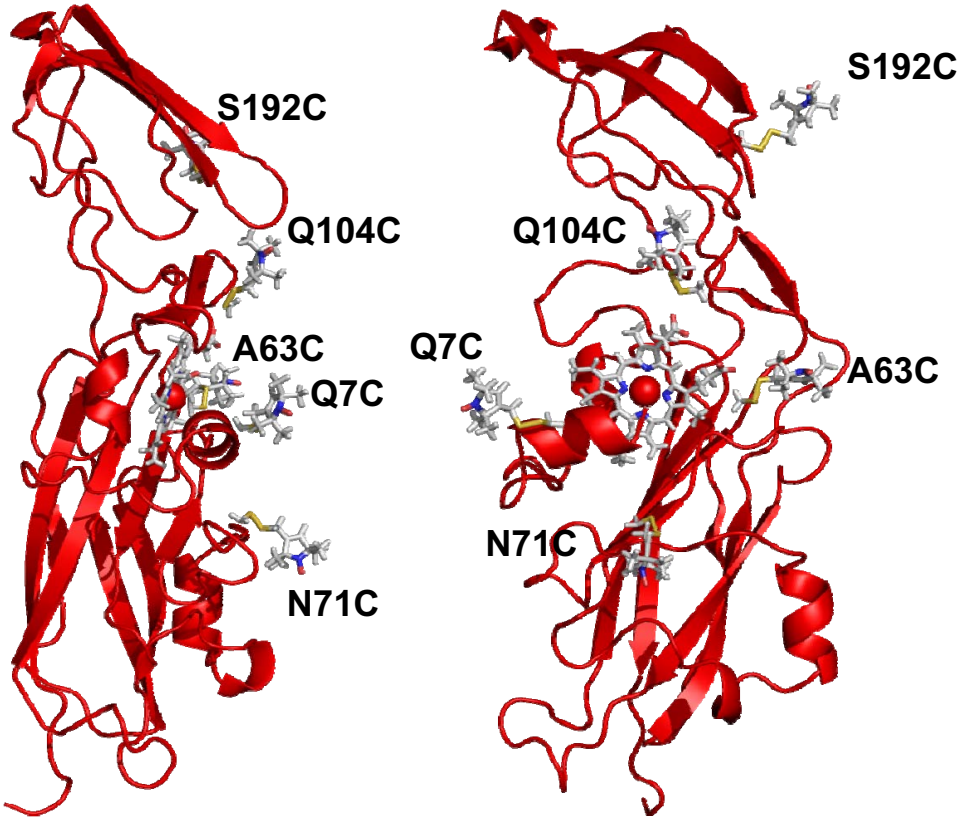

Figure 4.1. Positions of the MTSL spin labels on cyt*f*. The molecule on the right has been rotated over 90° relative to the one on the left.

The spin labels were attached to cyt*f* in order to induce an intermolecular paramagnetic relaxation enhancement (PRE) on amide nuclei of ^{15}N-M58C cytc_6. Cytc_6 is prone to autoreduction, which can lead to spin label reduction. Therefore, the M58C mutant variant of cytc_6 was used. Replacement of the Met58 Fe ligand with Cys causes a reduction of the midpoint potential of several hundred mV, yielding a variant with a midpoint potential of +265 mV (Dr. Lange, personal communication), that does not show any autoreduction. XRD analysis of wt and M58C cytc_6 showed that the crystal structures are almost identical with rmsd values of 0.16 and 0.23 Å for backbone and all heavy atoms (Dr. Pannu, personal communication).

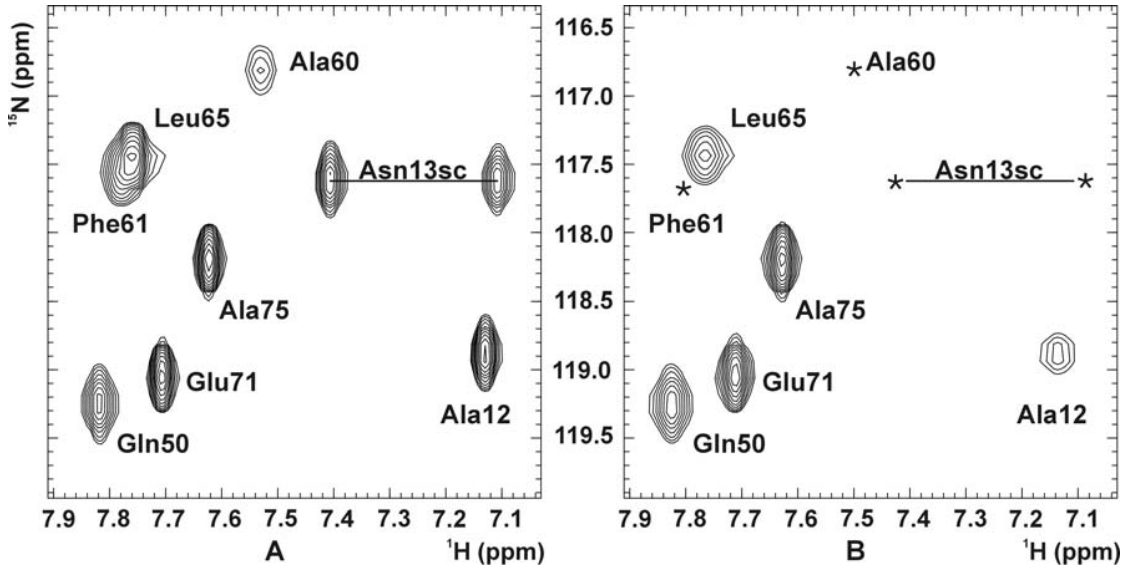

Figure 4.2. Part of the ^{1}H-^{15}N-HSQC spectrum of M58C cytc_6 in the presence of Q104C cyt*f* modified with A) diamagnetic spin label and B) paramagnetic spin label. The ratio ^{15}N M58C cytc_6 : cyt*f* is 3:1. Asterisks denote the position of peaks in A), which are no longer observed in B).

In five separate experiments the effect of paramagnetically labelled cyt*f* on the ^{1}H-^{15}N HSQC spectrum of ^{15}N-M58C cytc_6 was compared to the effect of diamagnetically labelled cyt*f*. When, for example, Q104C-cyt*f* is introduced a number of resonances in ^{15}N-M58C cytc_6 broaden out and several disappear entirely from the spectrum (Fig. 4.2). These effects are observed in the presence of the other four cyt*f* mutants as well. To ensure the labels themselves do not interfere with binding of cyt*f* to ^{15}N M58C cytc_6 the ^{1}H chemical shift changes brought about by the cyt*f*-MTS mutants are compared with the

^{1}H chemical shift changes in the unlabelled complex (Fig. 4.3). A similar pattern of chemical shift changes is observed for the unlabelled and MTS-labelled complexes, although small variations are noticeable. General scaling differences represent small differences in fractions bound between experiments with spin labelled cyt*f*. These were taken into account by the use of a scaling factor in docking calculations (see below).

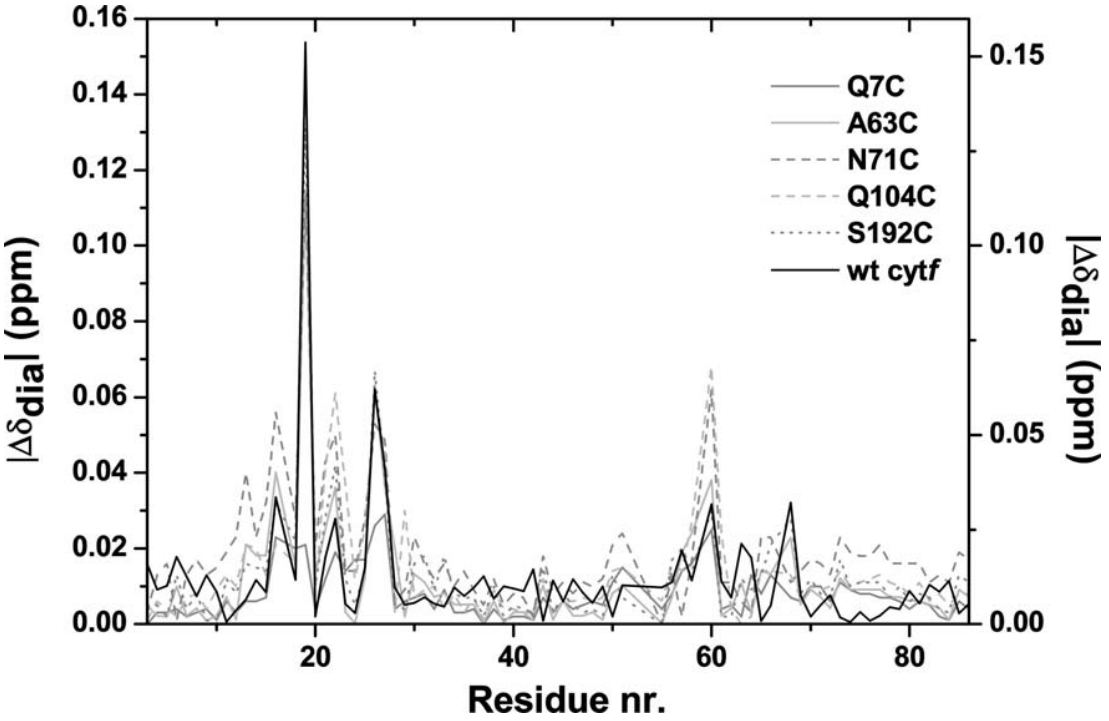

Figure 4.3. ^{1}H chemical shift changes observed at 3:1 ^{15}N M58C cytc_6: cyt*f*-MTS for all five cyt*f* mutants (left y-axis) and for the 1:3 ^{15}N M58C cytc_6 : cyt*f* complex (right y-axis).

It can be concluded that the observed changes in intensity are caused by an increase in the relaxation rate ($R_{2,\ para}$) of the affected protons, due to their proximity to the unpaired electrons of MTSL. PRE effects are distance dependent and they were converted into five sets of restraints for docking. Rigid-body calculations with all possible combinations of three pairs of these sets have been performed. It was observed that all these runs converge strongly towards a single structure. Also, when all five sets of restraints together were used a single structure is found.

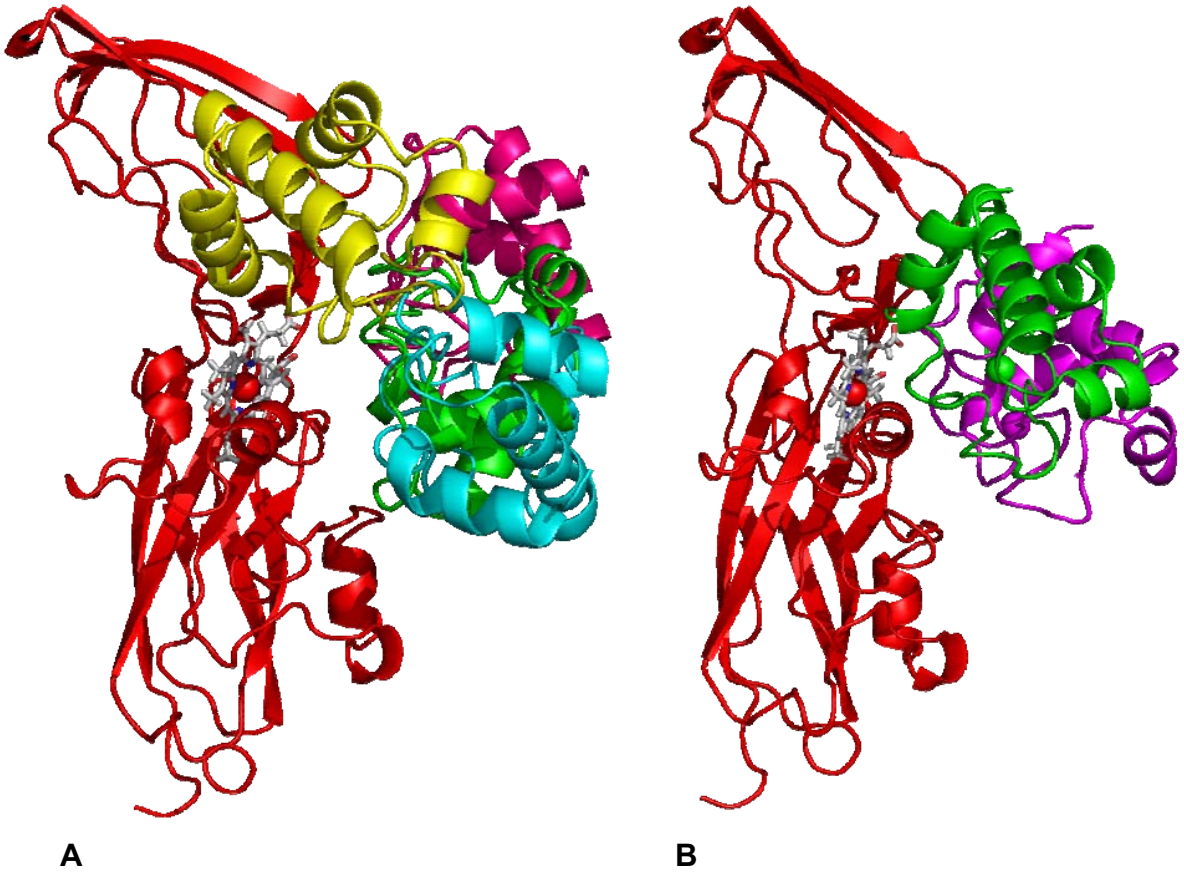

Figure 4.4. A) Overlay of structures of the M58C cytc_6 - cyt*f* complex determined by docking with distance restraints from all five spin labels (green), spin labels Q7C, A63C and Q104C (cyan), Q7C, A63C and S192C (yellow) and A63C, N71C and S192C (pink). B) Overlay of the structures determined with chemical shifts perturbation data as restraints (magenta) and chemical shifts perturbation data and PCS as restraints (dark green).

From an overlay of several of these structures (Fig. 4.4A), it is evident that the positions and orientations of cytc_6 to cyt*f* diverge remarkably between the different spin label sets used. This can also be concluded from the violations summarised in Table 4.2. The spin labels corresponding to the sets of restraints that are not used in a particular docking show a higher number of violated residues and a larger average distance violation. When all five sets of restraints are used, the average distance violations are more evenly distributed over the restraints sets. The spin label attached to S192C on cyt*f,* furthest away from the haem, generally has high average distance violations from a relatively

small number of violated residues. The observations from docking with PRE derived restraints suggest it is not possible to meet all restraints in a single structure. Similarly, the previously published structure determined by docking with chemical shift data[135] and a structure previously determined by docking with chemical shift perturbation and PCS data together (Fig. 4.4B) (Dr. Irene Díaz-Moreno, personal communication) demonstrate the variability in results obtained from docking with various types of NMR data. When all these NMR data are considered it is likely that dynamics play a role in complex formation between cytc_6 and cyt*f*.

Table 4.2. Statistics on distance violations for the lowest energy structures of M58C cytc_6 – cyt*f*-MTSL complexes from docking with restraints from all 5 spin labels (5SL) and all combinations of 3 spin labels (numbers indicate position of spin label on cyt*f*). The number of violated residues (Nr.) and the average distance violation (Av.) are shown for each spin label (SL). The statistics for spin labels which were excluded from a particular combination are shown in bold.

Docking:	**5SL**		**7/63/71**		**7/63/104**		**7/63/192**		**7/71/104**		**7/71/192**	
SL	Nr.	Av.	Nr.	Av.	Nr.	Av.	Nr.	Av.	Nr.	Av.	Nr.	Av.
Q7C	23	5.7	20	5.5	18	2.5	26	3.8	21	3.3	29	5.1
A63C	38	2.1	18	2.7	30	2.5	28	3.1	**46**	**4.5**	**65**	**5.3**
N71C	32	2.0	15	3.6	**32**	**7.0**	**39**	**8.1**	36	3.0	25	3.2
Q104C	34	4.8	**35**	**4.4**	23	3.3	**24**	**10.7**	23	3.3	**26**	**8.2**
S192C	12	9.4	**12**	**13.1**	**14**	**16.6**	12	9.8	**11**	**14.9**	12	5.5
Total	139	4.8	100	5.9	117	6.4	129	7.1	137	5.8	157	5.5

Docking:	**7/104/192**		**63/71/104**		**63/71/192**		**63/104/192**		**71/104/192**	
SL	Nr.	Av.	Nr.	Av.	Nr.	Av.	Nr.	Av.	Nr.	Av.
Q7C	20	3.2	**30**	**5.1**	**26**	**13.7**	**19**	**8.4**	**36**	**6.1**
A63C	**60**	**5.7**	21	2.2	23	2.9	22	2.1	**60**	**6.0**
N71C	**49**	**5.6**	26	3.0	32	2.1	**27**	**2.0**	12	2.8
Q104C	20	6.2	43	3.9	**26**	**13.2**	23	6.2	29	5.0
S192C	20	5.6	**12**	**13.7**	10	5.1	12	8.1	14	6.7
Total	169	5.3	132	5.6	117	7.4	103	5.4	151	5.3

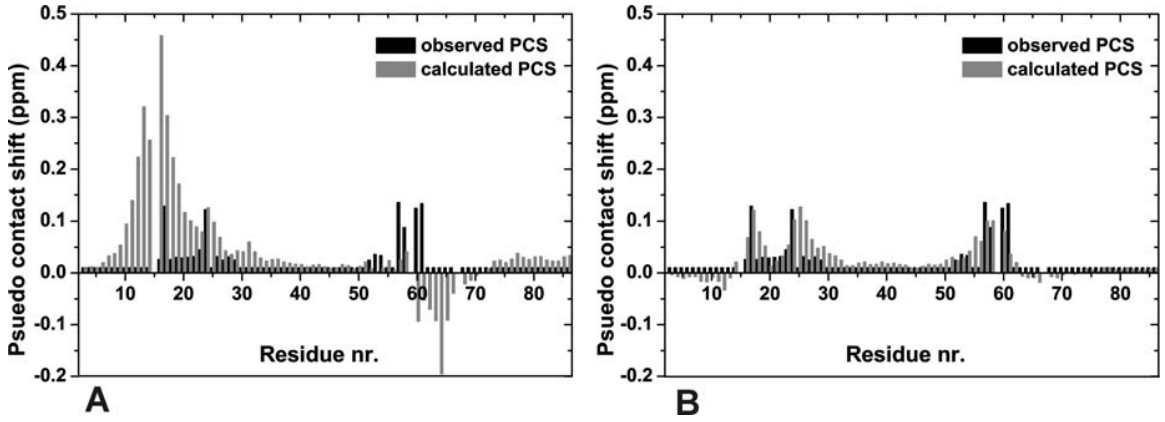

Figure 4.5. Observed and calculated ^{1}H PCS for the structure of the M58C cytc_6 – cyt$f$ complex determined with A) chemical shifts perturbation data as restraints and B) chemical shifts perturbation data and PCS as restraints. All non-significant PCS are indicated with a bar of 0.01 ppm.

Dynamics simulations

When the PCS are back-calculated for both structures in Figure 4.4B and compared to the observed PCS it is clear that the PCS data improve the structure of the cytc_6 - cyt$f$ complex (Fig. 4.5). In order to determine if increased dynamics in the M58C cytc_6 - cyt$f$ complex can result in both the observed PCS and PRE simultaneously, simulations were performed. For comparison, the orientation of the protein in the structure based on chemical shift data[135] and the structure based on chemical shift and PCS data together were used as a starting point.

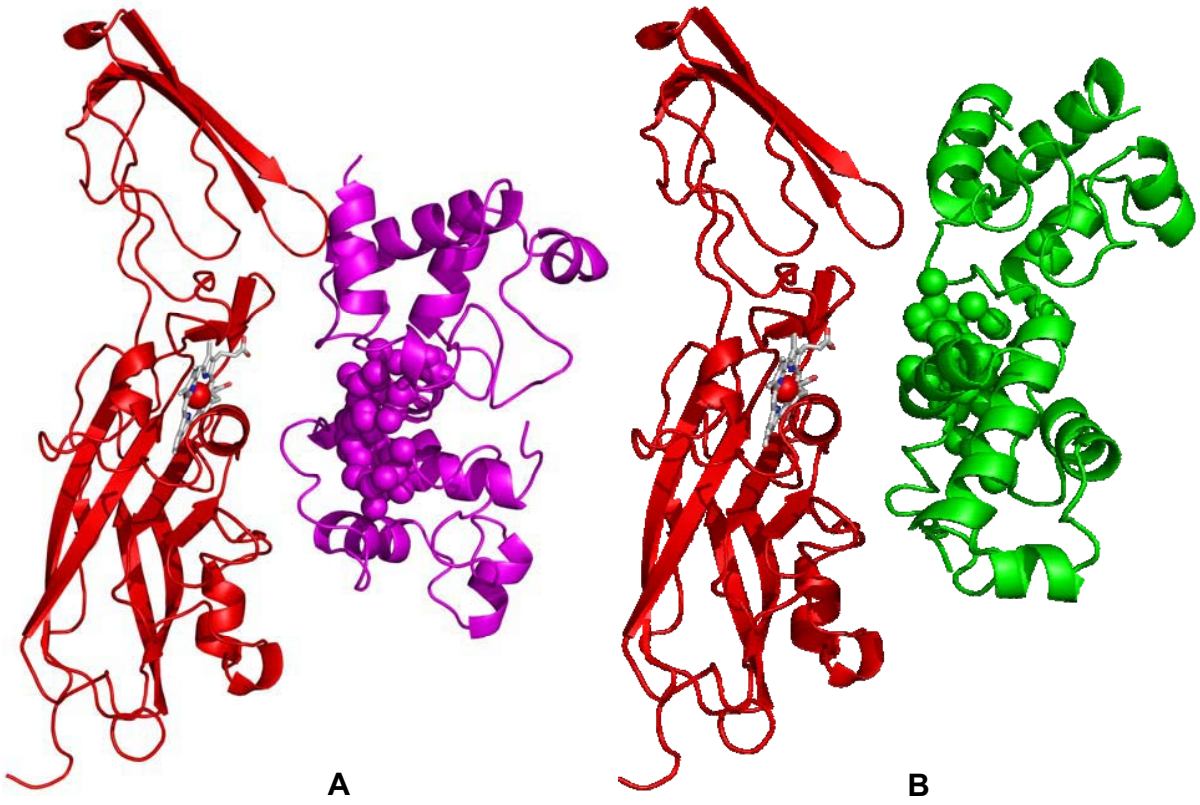

Figure 4.6. Representation of the dynamics in the M58C cytc_6 – cyt*f* complex. The starting position for the random rotations is found by A) docking with chemical shift changes or B) docking with chemical shift changes and PCS. The Fe in a set of fifty M58C cytc_6 molecules is shown as A) magenta or B) green spheres. The two most extreme orientations of M58C cytc_6 are shown as ribbons. Cyt*f* is shown as a red ribbon with the haem in sticks and the Fe ion as a sphere.

Random rotation of M58C cytc_6 around the Fe-Tyr1 N axis within the range of 30º, 30º and 90º in the x-, y- and z-direction, respectively, combined with random rotation around the centre of mass of M58C cytc_6 (wobble) of up to 60º in all directions (Fig. 4.6) was found to be in best agreement with the observed data. As shown in Chapter III, these simulations cannot determine which set of variables represents the actual movements found in the complex, but give an indication of the minimal amplitude. PCS violation analysis of the averaged PCS in the simulated ensemble of 50 positions indicates that when the structure determined with PCS data is used as starting position for the random rotations, the averaged PCS match quite well the observed PCS (Fig. 4.7). However, comparison with PCS calculated from the single orientation structure (Fig. 4.5B**)** shows that this way of creating an ensemble does not improve the match between observed and

calculated PCS in the ensemble. When the structure determined with just chemical shift data is considered the averaged PCS deviate, especially for the first twenty residues. The binding interface in both structures is similar, but the PCS probably refine the orientation of cytc_6 towards the haem in cyt*f*.

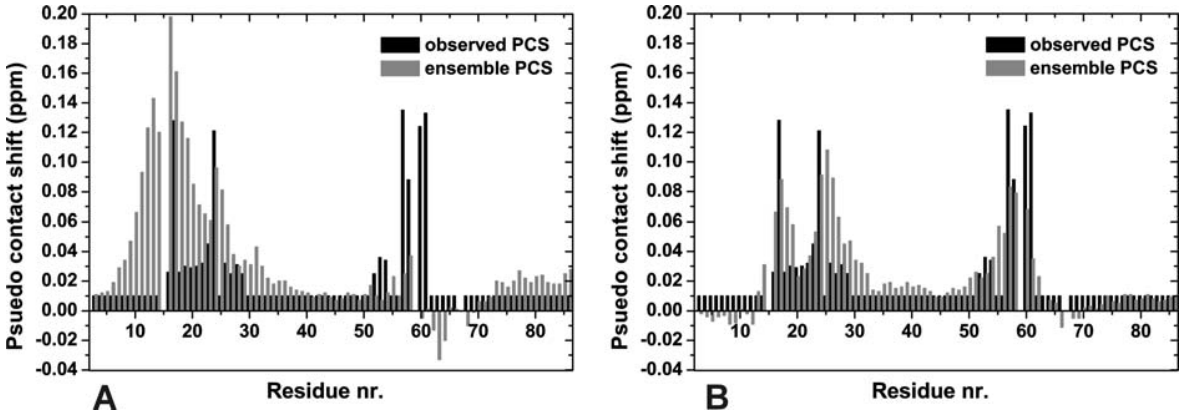

Figure 4.7. Observed and averaged, simulated ^{1}H PCS for the ensemble generated around the structure of the M58C cytc_6 – cyt*f* complex determined with A) chemical shifts perturbation data as restraints and B) chemical shifts perturbation data and PCS as restraints. All non-significant PCS are indicated with a bar of 0.01 ppm

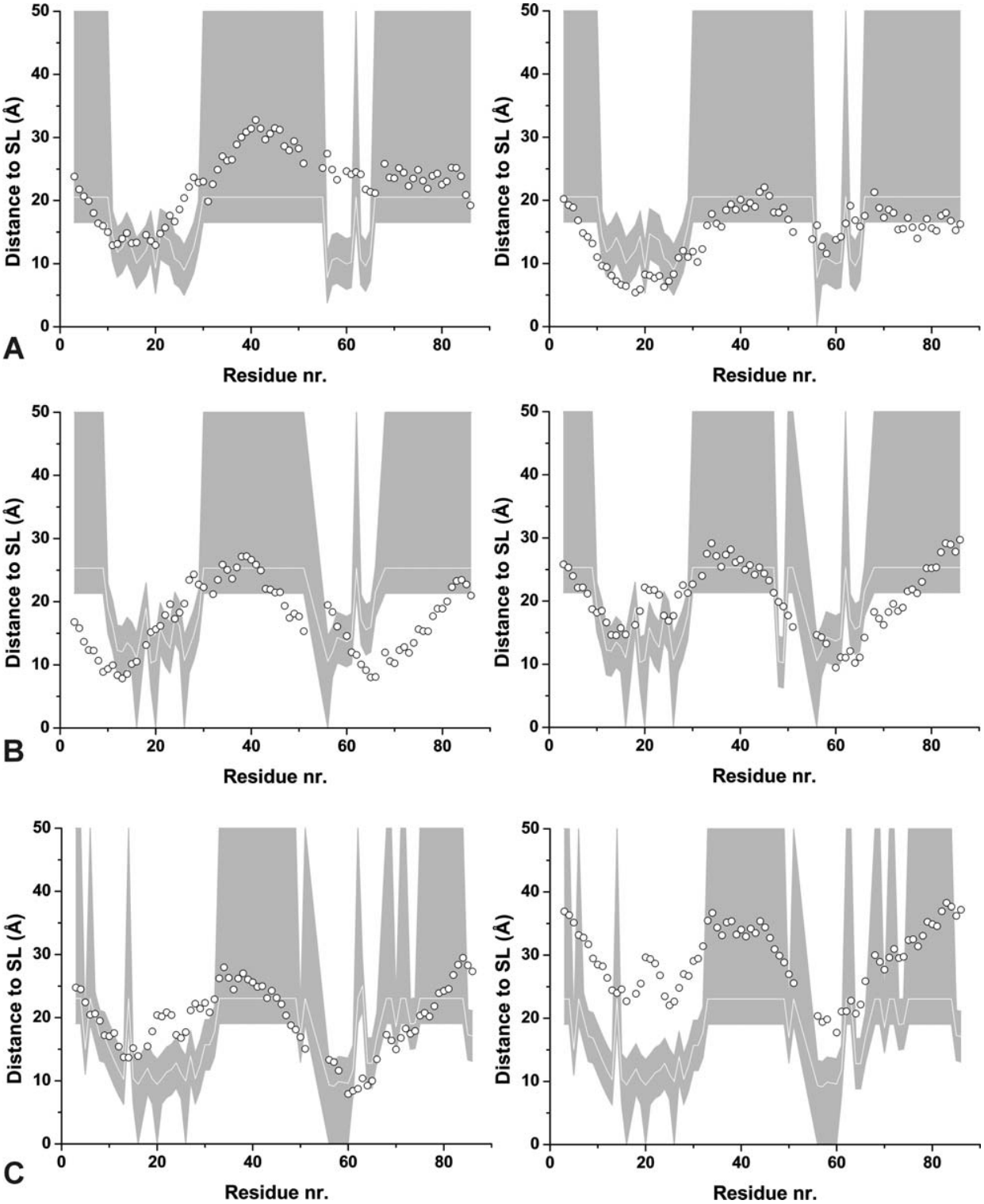
A
B
C
Distance to SL (Å)
Residue nr.
0
10
20
30
40
50
0
20
40
60
80

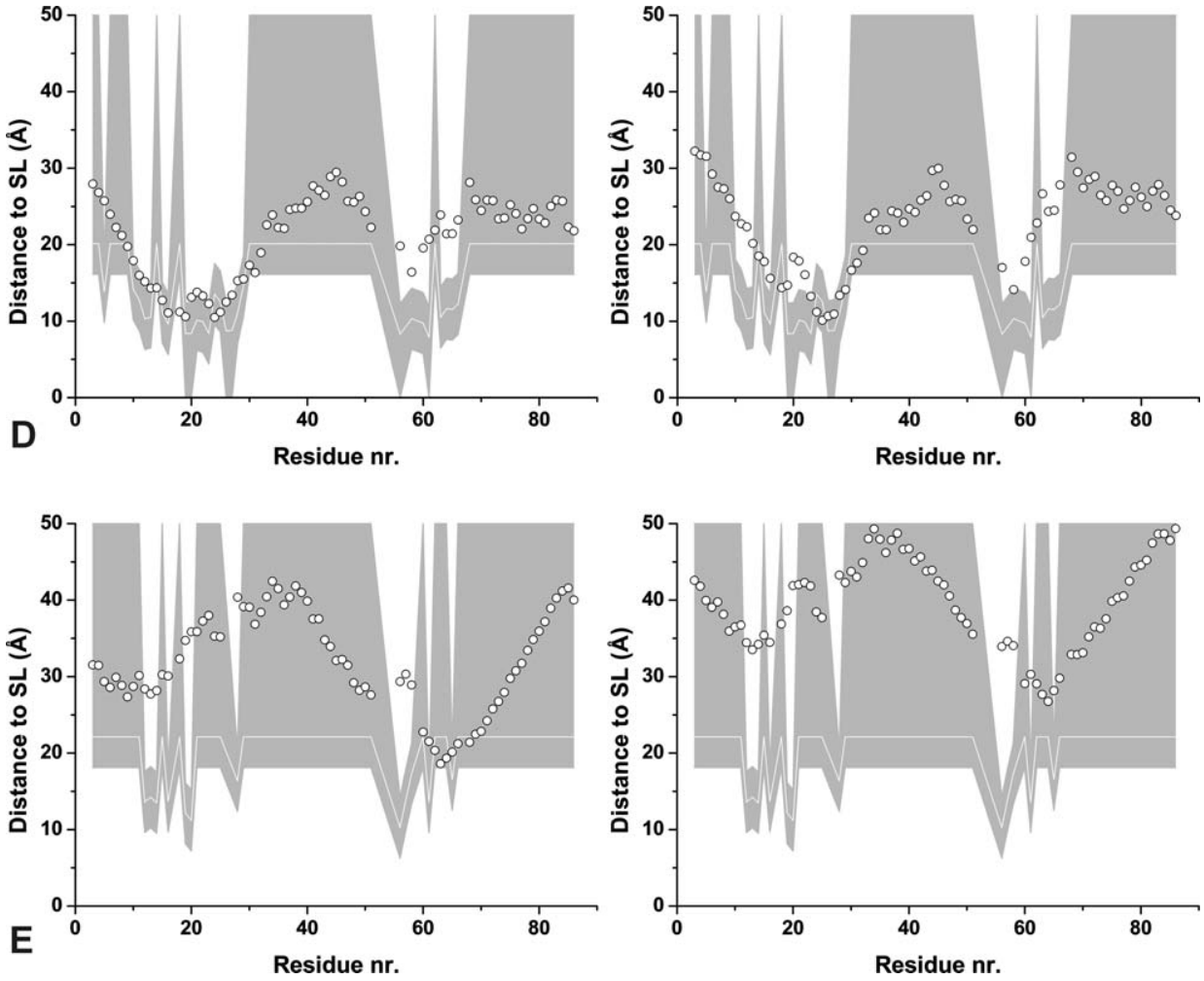

Figure 4.8. Ensemble averaged distances of residues in M58C cytc_6 to spin label at A) Q7C, B) A63C, C) N71C, D) Q104C and E) S192C on cyt*f*. On the left of every panel the ensemble with random rotations around the position of M58C cytc_6 found by docking with chemical shift changes and on the right the ensemble around the position found by docking with chemical shift changes and PCS. The grey area represents the allowed area for each residue and the white line the experimentally determined, PRE-derived distances used as input in docking. Open circles denote r^{-6} averaged distances for an ensemble of 50 structures.

Violations of distances derived from PRE for all five spin label positions are shown for the two ensembles created around the two starting structures (Fig. 4.8). These violations remain large (Table 4.3), indicating that the simple model used here to simulate movement in the complex does not account for all PRE effects observed. This is most obvious for the spin label S192C, furthest away from the haem. For both starting structures, when the S192C spin label is considered, only a few residues are actually violated but the average violation distance is notably larger than for the other spin labels. This indicates that cytc_6 spends more time close to this spin label than simulated here. It is concluded that the ensemble must have an uneven distribution, with certain preferred orientations. The approach to create an ensemble of randomly rotated orientations based on a single starting position appears unsuitable to sample all the dynamics in this complex, contrary to what was found for the Pc - cyt*f* complex of *P. hollandica* (Chapter III).

Table 4.3. Statistics on distance violations for simulated ensemble of cytc_6 – cyt*f* complexes. The total number of restraints is shown in parenthesis.

	Chem. shift based structure		**Chem. shift and PCS based structure**	
Spin label	Nr. of violated residues	Avg. violation (Å)	Nr. of violated residues	Avg. violation (Å)
Q7C	17 (90)	6.6	38 (90)	1.6
A63C	28 (88)	3.1	31 (88)	3.2
N71C	30 (89)	3.7	38 (89)	7.5
Q104C	15 (88)	4.6	20 (88)	5.8
S192C	12 (87)	14.1	12 (87)	17.3
Total	102 (442)	6.4	139 (442)	7.1